

Article

Oil-Air Distribution Prediction Inside Ball Bearing with Under-Race Lubrication Based on Numerical Simulation

Yaguo Lyu , Yuanhao Li ^{*}, Can Li, Le Jiang and Zhenxia Liu

School of Power and Energy, Northwestern Polytechnical University, Xi'an 710129, China; yglu@nwpu.edu.cn (Y.L.); lican2024@mail.nwpu.edu.cn (C.L.); ljiang@mail.nwpu.edu.cn (L.J.); zxliu@nwpu.edu.cn (Z.L.)

* Correspondence: liyuanhao0403@mail.nwpu.edu.cn

Abstract: Oil/air two-phase flow distribution in the bearings is the basis for bearing lubrication status identification and precise thermal analysis of the bearing. In order to understand the fluid behavior inside the under-race lubrication ball bearing and obtain an accurate oil volume fraction prediction model. A numerical study of ball bearing with under-race lubrication is carried out to study oil-gas two-phase distribution inside the bearing, and the influence of several parameters is quantified, like bearing rotating speed, oil flow rate, oil viscosity, and oil density. The results indicate that the oil fraction in the bearing cavity between the inner and outer ring shows a periodic distribution along the circumference direction, and the period is the same as the number of under-race oil supply holes. Oil distribution along radial direction is affected by the outer-ring-guiding cage and centrifugal force, leading to oil accumulation near the outer ring. Different bearing running conditions and oil characteristics do not change the oil distribution trend along circumference and radial direction, but the difference ratio. Finally, based on the numerical simulation results, a formula for the average oil volume fraction prediction in the bearing ring cavity is constructed.

Keywords: ball bearing; under-race lubrication; two-phase flow; aero-engine; computational flow dynamics



Citation: Lyu, Y.; Li, Y.; Li, C.; Jiang, L.; Liu, Z. Oil-Air Distribution Prediction Inside Ball Bearing with Under-Race Lubrication Based on Numerical Simulation. *Appl. Sci.* **2024**, *14*, 3770. <https://doi.org/10.3390/app14093770>

Academic Editor: Nicola Pio Belfiore

Received: 18 March 2024

Revised: 16 April 2024

Accepted: 25 April 2024

Published: 28 April 2024



Copyright: © 2024 by the authors. Licensee MDPI, Basel, Switzerland. This article is an open access article distributed under the terms and conditions of the Creative Commons Attribution (CC BY) license (<https://creativecommons.org/licenses/by/4.0/>).

1. Introduction

The high-speed roller bearing is the core of the main shaft supporting the structure of high-speed rotating machines like aero-engine, and its stable and reliable operation is crucial to ensure the normal operation of the entire engine [1]. With the improvement of the thrust-to-weight ratio and economy performance of aero-engines, the main-shaft rotating speed is also increasing, leading to a higher bearing DN (rotating speed (rpm) × inner diameter (mm)) value and larger bearing heat generation [2]. The challenges of bearing lubrication and cooling are increasing in the bearing and oil system design. Oil shortages lead to insufficient lubrication, increased mechanical friction, bearing overheating, and even oil ignition [3]. On the contrary, too much oil supply could not only increase the system weight and load but also cause severe fluid viscous friction [4]. Therefore, it is necessary to accurately understand the behavior of oil within the bearing so as to complete the precise design of the lubrication system and main-shaft bearing lubrication scheme and ensure the performance, lifespan, and reliability of the aero-engine.

Traditionally, the main-shaft roller bearing in aero-engines commonly uses jet lubrication [5]. However, as the bearing DN value increases, the centrifugal force, together with high-speed rotating rolling elements, makes it difficult for the oil to enter the bearing cavity [6], so under-race lubrication is developed. In under-race lubrication, oil is ejected from several nozzles and carried by oil scoops connecting with the inner ring. With centrifugal force caused by high-speed rotation, oil is supplied into the bearing cavity through radial holes on the inner ring, achieving lubrication and cooling of the bearing. Compared to

jet lubrication, under-race lubrication provides better lubrication and cooling effects for high-speed conditions and has been increasingly adopted in modern aero-engine [7].

In high-speed roller bearings, the interaction between the lubricating fluid and the moving elements causes complex oil-gas two-phase flow within the bearing cavity [8]. Many scholars have conducted extensive research on this topic. As early as 1974, Zaretsky et al. [9] experimentally studied the operating characteristics of ball bearings with contact angles of 20° and 24° under DN values of 3.0×10^6 . The results showed that with the increase in the total amount of lubricant oil and inner ring cooling flow, the temperatures of both the inner and outer rings of under-race lubrication bearings significantly decreased. Pinel et al. [10,11] conducted an experimental study on the operating characteristics of ball bearings and cylindrical roller bearings with under-race lubrication. They found a good correlation between the predicted power loss values and the experimental test values. Parker [12] indirectly derived an estimation expression for the average oil volume percent inside the ball bearing with jet lubrication based on experimental studies of thermodynamic characteristics. Cavallaro et al. [13] modified Parker's [12] formula for under-race lubrication conditions, taking into account the rotating speed of oil and changing the inner ring rotating speed to the relative speed between the cage and inner ring. Hu et al. [14] used the CFD method to study the oil-gas two-phase flow in the jet lubrication ball bearing. They found that the oil phase distribution inside the bearing is uneven. The increase in rotating speed would decrease the average oil phase volume fraction, whereas the effect of the oil flow rate is adverse. Liebrecht et al. [15] investigated the influence of the location of oil on the total friction torque of a roller bearing with a vertical rotating axis. Zhang et al. [16] found that as the jet velocity increases, the churning torque decreases, while as the bearing speed increases, the churning torque increases. Adeniyi et al. [17] used numerical simulations to study the oil and gas flow between the bearing inner race and the cage. After leaving the oil inlet hole, the oil forms a wetting area on the inner surface of the bearing cage, spreading and falling off to both sides. Wu et al. [18] studied the flow field and temperature distribution of jet lubrication ball bearings by numerical simulation and experiment. The temperature distribution is affected by the oil volume fraction, and the higher temperature appears at the position where the oil volume fraction is lower. Yan et al. [19] used the CFD method to analyze the oil-gas two-phase flow in ball bearings. Compared with the single nozzle structure, the temperature and pressure of the double nozzle bearing cavity are relatively low, and the airflow mode of the double nozzle is more complicated. Gao et al. [20] used the CLSVOF multiphase flow method to track the oil/air two-phase flow inside the under-race lubrication roller bearing and obtained the influence of various factors. The results show that there is an optimal oil inlet velocity to maintain more oil accumulation in the bearing cavity. Jiang et al. [21] studied the oil-air two-phase flow inside the under-race lubrication ball bearing through CFD simulation and found that the diffusion degree of oil on the outer ring, cage, ball, and inner ring decreased in turn. Optimizing the oil inlet hole according to the average oil volume fraction helps to achieve accurate lubrication of under-race lubrication ball bearings.

In summary, in view of the complicated internal geometry of the bearing and its operating environment, research on fluid behavior inside under-race lubricating ball bearings is scarce and early-stage, and the understanding of oil-air two-phase flow inside the bearing cavity is very limited. The study of oil phase distribution in the bearing is helpful to study the heat transfer in the bearing. The accurate prediction model for oil volume fraction is beneficial to the optimization of the oil supplying flow rate for the bearing and bearing drag and churning loss estimation. As it is quite difficult to accurately obtain oil distribution and motion behavior in high-speed ball bearings through theoretical or experimental methods, the numerical simulation method is used in this article. Oil distribution characteristics along circumferential and radial directions inside the ball bearing with under-race lubrication are analyzed, as well as the influence of the bearing's running and lubricating conditions, such as bearing rotating speed, oil flow rate, oil viscosity, oil density on the oil distribution.

Finally, a suitable method for estimating the average oil volume percent in the bearing is established.

2. Model and Method

2.1. Geometric Model

The type of ball bearing used in this article is a deep groove ball bearing, as shown in Figure 1, including the inner ring, outer ring, spherical roller elements, and the outer ring guiding cage. The bearing material is generally steel. The specific dimensions of the bearing are shown in Table 1. There are 6 radial holes in the inner ring arranged uniformly in the circumference direction. These holes are located on the bottom of the inner ring raceway and have a diameter of 1 mm. Lubricating oil is supplied to the rotating shaft and flows into the bearing cavity through these radial holes in the inner ring with centrifugal force. Therefore, it is much easier for oil to enter the bearing with a higher rotating speed. But, because the oil does not only have radial motion but circular motion along with the inner ring, it's easier for it to escape from both ends of the bearing compared with jet lubrication in high-speed conditions.

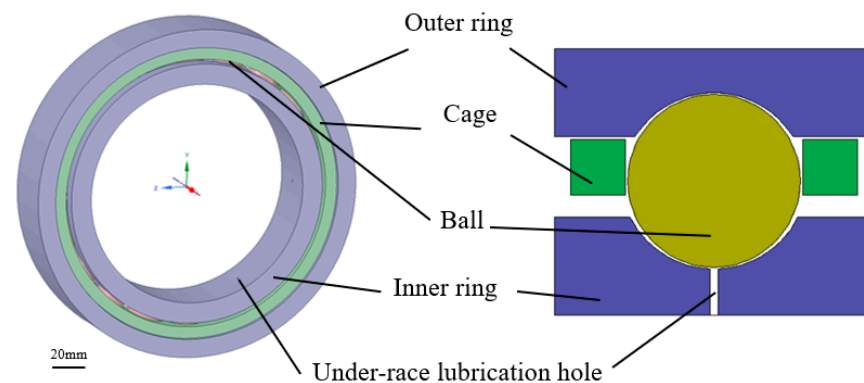


Figure 1. Geometric model of ball bearing.

Table 1. Structure parameters of the ball bearing.

Structure Parameters	Value
Outer race diameter	200 mm
Inner race diameter	133.35 mm
Pitch diameter	167 mm
Width	40 mm
Ball diameter	22 mm
Number of balls	20
Curvature coefficient of inner and outer raceways	0.52/0.515

2.2. Fluid Domain Meshing

In this article, to capture oil flow and distribution characteristics in bearing cavities with under-race lubrication, the fluid domain between the inner and outer rings is extracted, except the solid domain of spherical rollers and the cage. Besides, two circular fluid domains are added on both sides of the bearing to monitor the oil's splashing. On account of complex relative motion inside the bearing, the fluid domain is separated into four parts, as shown in Figure 2, including the hole region, the ball region, the main fluid region, and the external fluid region. The hole region has six radial cylindrical channels on the inner ring and rotates around the bearing center with the inner ring's rotating speed. The main fluid region is the cavity between the inner and outer ring, and it rotates with the cage speed to represent the rollers' revolution. The ball region consists of 20 hollow spherical domains with one homocentric roller in each one. The ball region revolves together with the main fluid region and rotates by its own rotating axis (the connection line of two roller-raceway

contact points) at the same time. The extended external fluid region is located on both sides of the main fluid region to provide a reasonable boundary environment for the oil-air two-phase flow simulation.

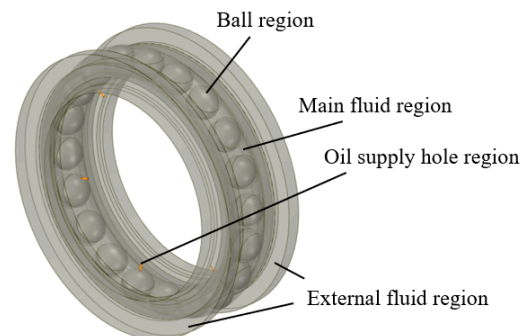


Figure 2. Ball bearing fluid domain.

The software ANSYS2020R1 Mesh is employed to discretize the fluid domain in ball bearing with under-race lubrication, as shown in Figure 3. Due to the complex internal structure of the bearing, the entire fluid region is meshed using tetrahedral unstructured mesh, and the slit in the contact zone is locally refined to improve the mesh quality, such as the contact zones between balls and inner ring, balls and outer ring, balls and the cage, and the cage and guide face.

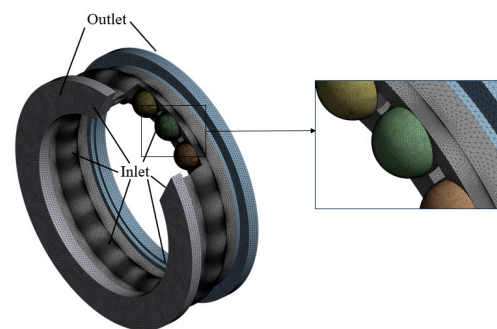


Figure 3. Computational mesh structure and boundary condition.

In order to exclude the influence of the guiding model on simulation results, three different mesh models are compared for independence determination. The oil volume fraction inside the bearing is analyzed, and the result is listed in Table 2. The bearing rotating speed is 5000 rpm, with an oil flow rate of 3 L/min, oil viscosity of 0.0046 Pa·s, and oil density of 938.6 kg/m³. It could be found that the calculated results are similar, and to ensure calculation accuracy with acceptable computational cost, a mesh with 3,143,919 cells and 598,702 nodes is selected.

Table 2. Mesh independence verification.

Number of Grids	Oil Volume Fraction
2,286,395	0.0133
3,143,919	0.0135
4,164,156	0.0136

2.3. Two-Phase Flow Model

The VOF model is used to capture the complex oil-air two-phase distribution characteristics in the under-race lubrication ball-bearing cavity. It uses a volume fraction function to represent the location of different fluid-free surfaces and the volume occupied by different fluids, better capturing the interface between different phases [22]. In the VOF method, a

volume fraction φ_{oil} is used to define the oil phase volume fraction; the volume fraction of the air phase is $(1 - \varphi_{oil})$. If $\varphi_{oil} = 1$, it means that the cell is full of oil; if $\varphi_{oil} = 0$, it means that the cell is full of air; if $0 < \varphi_{oil} < 1$, it means that the cell is in an oil-air two-phase mixing state. The volume fraction φ_{oil} can be solved by the following equation:

$$\frac{\partial}{\partial t}(\varphi_{oil}\rho_{oil}) + \nabla(\varphi_{oil}\rho_{oil}\mu_{oil}) = S_{\alpha_{oil}} + (\dot{m}_{oa} - \dot{m}_{ao}) \tag{1}$$

where ρ_{oil} is the oil density, \dot{m}_{oa} is the mass transfer rate from the oil phase to the gas phase per unit volume, \dot{m}_{ao} is the mass transfer rate from the gas phase to the oil phase per unit volume, and $S_{\alpha_{oil}}$ is the source term defined by the volume fraction equation. The relationship between the volume fractions of the oil phase and gas phase is as follows:

$$\varphi_{oil} + \varphi_{air} = 1 \tag{2}$$

The equivalent density and viscosity of oil-gas two-phase can be expressed as follows:

$$\rho = \varphi_{oil}\rho_{oil} + (1 - \varphi_{oil})\rho_{air} \tag{3}$$

$$\mu = \varphi_{oil}\mu_{oil} + (1 - \varphi_{oil})\mu_{air} \tag{4}$$

2.4. Turbulence Model

The components in the ball bearing have a relatively high-velocity difference when rotating at high speed, which will form complex turbulent flows in the bearing. Due to the influence of factors such as large curvature flow and high strain rate inside the bearing, the RNG κ - ϵ turbulence model is adopted [23]. The RNG κ - ϵ turbulence model adapts well to the VOF model. The turbulent kinetic energy and dissipation rate equations are as follows:

$$\frac{\partial}{\partial t}(\rho k) + \frac{\partial}{\partial x_i}(\rho k \mu_i) = \frac{\partial}{\partial x_j} \left[\alpha_k \mu_{eff} \frac{\partial k}{\partial x_j} \right] + G_k - \rho \epsilon \tag{5}$$

$$\frac{\partial}{\partial t}(\rho \epsilon) + \frac{\partial}{\partial x_i}(\rho \epsilon \mu_i) = \frac{\partial}{\partial x_j} \left[\alpha_\epsilon \mu_{eff} \frac{\partial \epsilon}{\partial x_j} \right] + C_{1\epsilon} G_k \frac{\epsilon}{k} - \rho C_{2\epsilon} \frac{\epsilon^2}{k} \tag{6}$$

Among them:

$$\mu_{eff} = \mu + \mu_t \tag{7}$$

$$\mu_t = \rho C_\mu \frac{k^2}{\epsilon} \tag{8}$$

where k is turbulent kinetic energy, ϵ is turbulent dissipation, μ_i is time-averaged velocity, G_k is the generation of turbulent kinetic energy due to mean velocity gradients, μ_{eff} is effective dynamic viscosity, μ_t is turbulent viscosity, $C_{1\epsilon}$, and $C_{2\epsilon}$ are constant terms.

2.5. Revolution and Self-Rotation Speed

When the bearing is in motion, the outer ring is stationary, and the inner ring rotates, while the balls have both revolution and self-rotating speed. The oil supply hole speed is the same as the inner ring speed, while the main flow region and ball revolution speed are the same as the cage speed. The cage speed is as follows [24]:

$$n_m = \frac{n_i}{2} \left(1 - \frac{D \cos \alpha}{d_m} \right) \tag{9}$$

The rotating speed of the cage relative to the inner ring:

$$n_{mi} = n_m - n_i \tag{10}$$

Assuming that there is no serious sliding at the contact between the inner ring raceway and the ball, the linear velocity of the ball at the contact point should be equal to the linear velocity of the raceway:

$$v_m = \frac{1}{2}\omega_m d_m \left(1 - \frac{D \cos \alpha}{d_m}\right) = \frac{1}{2}\omega_r D \quad (11)$$

Since n is proportional to ω , and the Formula (10) is substituted into:

$$n_r = (n_m - n_i) \frac{d_m}{D} \left(1 - \frac{D \cos \alpha}{d_m}\right) \quad (12)$$

Substituting Formula (9) into Formula (12), the self-rotation speed of the balls is as follows:

$$n_r = \frac{d_m n_i}{2D} \left[1 - \left(\frac{D \cos \alpha}{d_m}\right)^2\right] \quad (13)$$

where n_m is the cage speed; n_i is the inner ring speed; D is the diameter of the ball; α is the contact angle; d_m is the pitch diameter; n_r is the ball's self-rotation speed; n_{mi} is the rotating speed of cage relative to inner ring; v_m is the cage linear velocity; ω_m is the cage angular velocity; ω_r is the ball angular velocity.

2.6. Numerical Method

The software ANSYS2020R1 Fluent is used to investigate the complicated oil–air two-phase flow inside the under-race lubrication ball bearing. In numerical calculations, the inlet boundary of the computational region is set as a velocity inlet condition, and the outlet boundaries on both sides of the bearing are set as pressure outlet boundary conditions. Two assumptions in the calculation process are isothermal conditions and hydrodynamics. The sliding mesh method is used to simulate the motion of various regions inside the bearing. At initialization, the gas phase volume fraction of the entire bearing fluid region is set to 1, and the oil phase volume fraction is set to 0. Air is set as the main phase, and oil is set as the secondary phase. The type of lubricating oil is Mobil Jet Oil II. The SIMPLE algorithm is used for pressure-velocity coupling of the two-phase flow inside the bearing. The pressure term uses the PRESTO! format, and the momentum, turbulent kinetic energy, and turbulent dissipation rate are discretized using the upwind scheme. To avoid divergence issues that may occur during the solution of nonlinear equations, under-relaxation iteration is used. During the calculation process, the inlet and outlet flow rates of the flow field and the average oil phase volume fraction inside the bearing are monitored. When the difference in inlet and outlet flow rates is around 1% and the average oil volume fraction inside the bearing remains basically unchanged, it is considered as converged, and the calculation is stopped to determine the final result.

3. Results and Discussion

3.1. Distribution Characteristics of Oil and Gas Two-Phase Inside the Bearing

As shown in Figure 4, this is the flow streamline diagram of the moving fluid region inside the bearing obtained through analysis. The bearing rotating speed is 11,000 rpm, the oil flow rate is 3 L/min, the oil viscosity is 0.0046 Pa·s, and the oil density is 938.6 kg/m³. Due to the influence of the cage and ball, the oil enters the bearing and generates a vortex. Because the ball rotates at a high speed, the oil follows the rotation of the ball and centrifugal force to move from the cage pocket to the outer ring zone and finally exits from the end face.

As shown in Figure 5, the state of the oil-gas mixture and the oil phase accumulation process inside the bearing are presented at different times. The amount of oil inside the bearing gradually increases with time until it reaches a stable state. When the time is 0.0025 s, the oil has just entered the bearing, and there is still very little oil inside the bearing. As the time progresses to 0.01 s, the oil inside the bearing continues to accumulate. When the time reaches 0.04 s, the distribution of oil inside the bearing has stabilized. It

can also be observed from the figure that there is more oil phase distribution near the under-race oil supply holes, while there is less oil in other positions. The following will analyze in detail the characteristics of oil-gas two-phase distribution in the bearing ring cavity and the influence of different parameters.

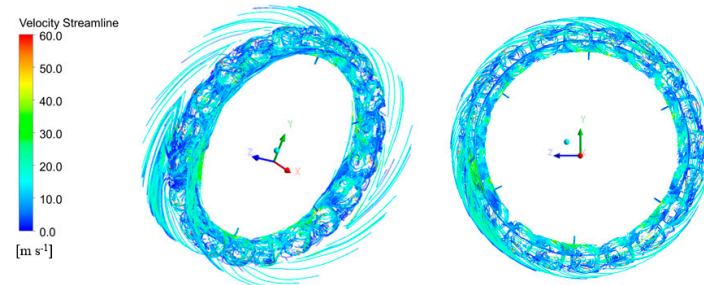


Figure 4. Streamlines diagram.

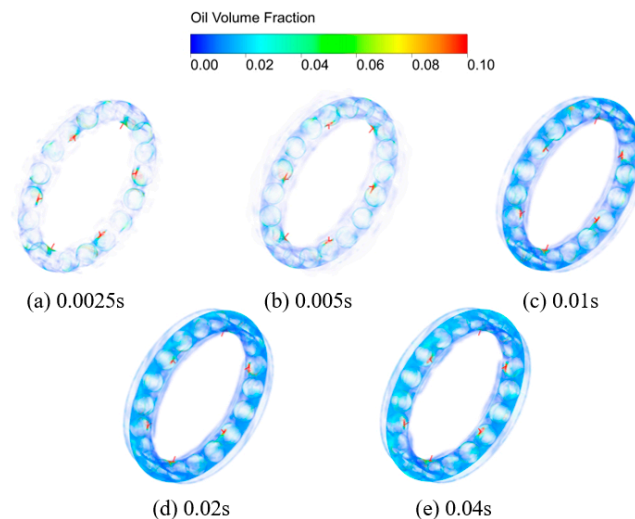


Figure 5. Oil distribution evolution inside the bearing with flow time.

3.2. The Effect of Bearing Rotating Speed

As shown in Figure 6, the oil-gas two-phase distribution cloud images inside the bearing at different bearing rotating speeds are presented. The oil flow rate is 3 L/min, the oil viscosity is 0.0046 Pa·s, and the oil density is 938.6 kg/m³. At different rotating speed conditions, the oil is mainly distributed near the outer ring of the bearing. With the increase of bearing rotating speed, the oil phase inside the bearing gradually decreases. Figure 7 shows the volume fraction of the oil phase inside the bearing along the circumference at different speeds. The oil exhibits periodic distribution in the bearing, with a period that is the same as the number of supply holes. The volume fraction of the oil phase is larger near the supply holes and smaller far away from them. With the bearing rotating speed increases, the rotating speed of the cage and ball also increases, resulting in a larger centrifugal force on the oil. The oil velocity inside the bearing becomes faster, making the oil distribution more uniform, but at the same time, the volume fraction of the oil phase decreases. Figure 8 shows the volume fraction of the oil phase inside the bearing along the radial direction at different rotating speeds. The oil mainly concentrates near the outer ring, which is consistent with the cloud image results shown in Figure 6. With the increase of the bearing rotating speed, the radial distribution of oil inside the bearing remains unchanged. Under the influence of increased bearing rotating speed, the centrifugal force on oil continues to increase. Under the guidance of the outer ring, it becomes easier for oil to be thrown to the outer ring rather than accumulate between the cage and inner ring, resulting in an increase in the volume fraction of the oil phase near the outer ring.

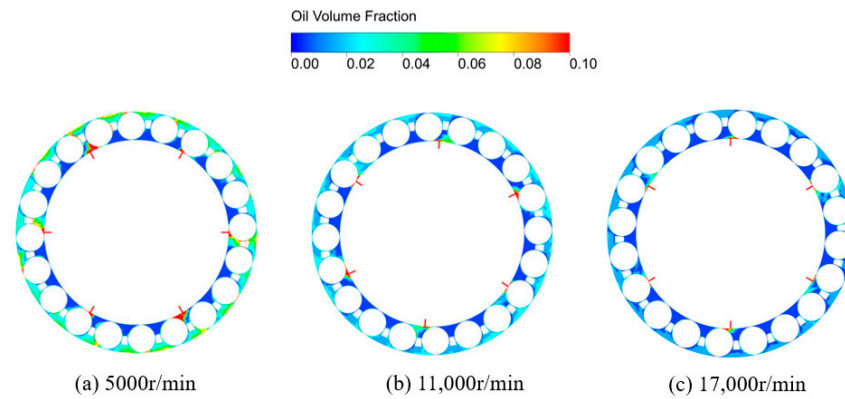


Figure 6. Oil and gas distribution at different bearing rotating speeds.

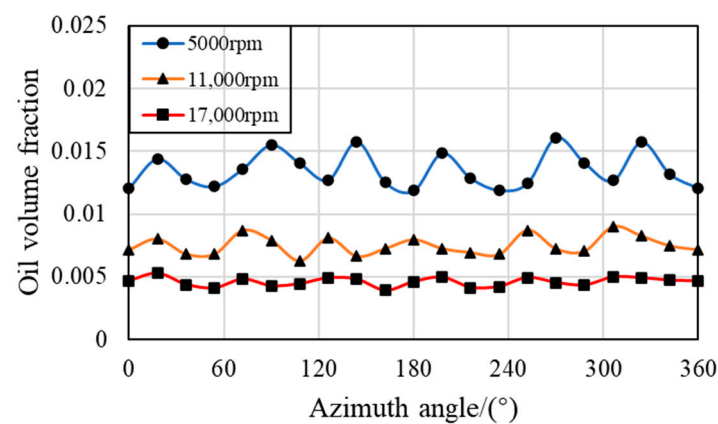


Figure 7. Circumferential oil volume fraction at different bearing rotating speeds.

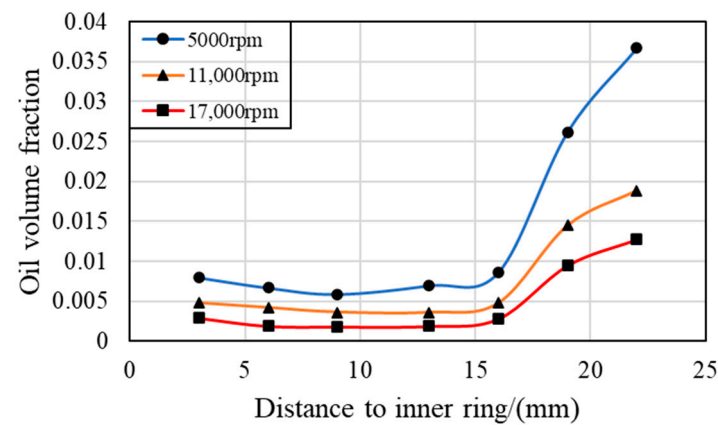


Figure 8. Radial oil volume fraction at different bearing rotating speeds.

As shown in Figure 9, the volume fractions of the oil phase near the inner and outer rings of the bearing, as well as the average oil phase volume fraction inside the bearing, are presented at different bearing rotating speeds. With the increase of bearing rotating speed, both the volume fractions of the oil phase near the inner and outer rings of the bearing decrease, and the average oil phase volume fraction inside the bearing decreases approximately linearly. When the bearing rotating speed increases from 5000 rpm to 17,000 rpm, the volume fraction of the oil phase near the inner ring of the bearing decreases by 66%, the volume fraction near the outer ring decreases by 69%, and the average oil phase volume fraction inside the bearing decreases by 66%. It can be seen that when the bearing rotating speed increases, the oil supply should be increased to ensure lubrication and cooling in the bearing.

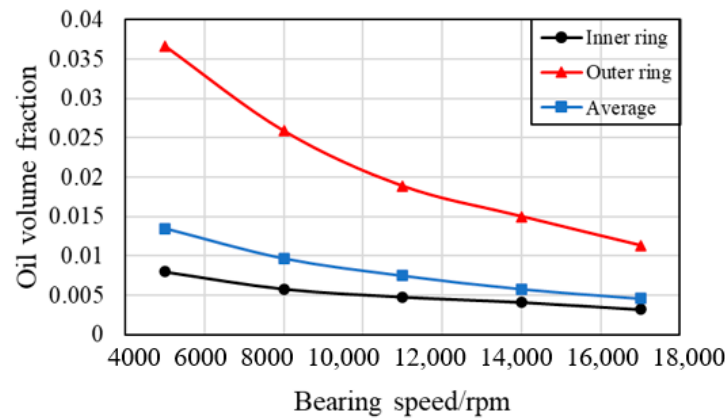


Figure 9. Oil volume fraction near the zone of the inner ring and outer ring at different bearing rotating speeds.

As shown in Figure 10, the ratio of oil phase volume fraction between the zone of outer and inner rings inside the bearing under different bearing rotating speeds is presented. With the increase of bearing rotating speed, the distribution difference of oil between the inner and outer rings decreases. When the bearing rotating speed is 5000 rpm, the volume fraction of the oil phase near the outer ring is approximately 4.59 times that near the inner ring. When the speed increases to 17,000 rpm, the volume fraction of the oil phase near the outer ring is 3.52 times that near the inner ring. This indicates that as the bearing rotating speed increases, the radial distribution of oil inside the bearing also tends to be more uniform.

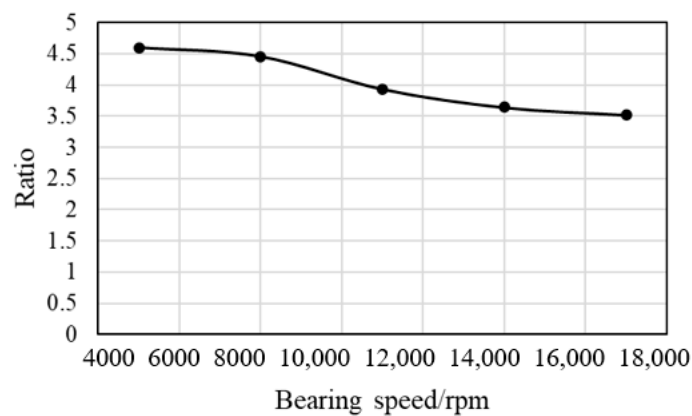


Figure 10. The ratio of oil volume fraction between the zone of outer and inner rings at different bearing rotating speeds.

3.3. The Effect of Oil Flow Rate

As shown in Figure 11, the oil-gas two-phase distribution inside the bearing at different oil flow rates is presented. The bearing rotating speed is 11,000 rpm, the oil viscosity is 0.0046 Pa·s, and the oil density is 938.6 kg/m³. With the increase in oil flow rate, the oil phase inside the bearing gradually increases, and it mainly concentrates near the outer ring. Figure 12 shows the volume fraction of the oil phase inside the bearing along the circumference at different oil flow rates. Under the action of the cage and balls, the oil gathered at the supply holes increases with the increase of the oil flow rate. The fluctuation of the oil volume fraction along the circumference increases, and the uniformity decreases. The radial distribution of oil inside the bearing remains unchanged, mainly concentrated near the outer ring (as shown in Figures 13 and 14). The distribution gap between the outer and inner rings of oil increases with the increase in flow rate, as shown in Figure 15. The decrease in the lubricating oil flow rate will lead to insufficient lubrication of bearings, and

it is difficult to take away the heat generated; the increase in oil flow rate will lead to an increase in fluid viscous friction. Therefore, for the oil flow rate, it is necessary to ensure lubrication while taking away the heat generated by the bearing.

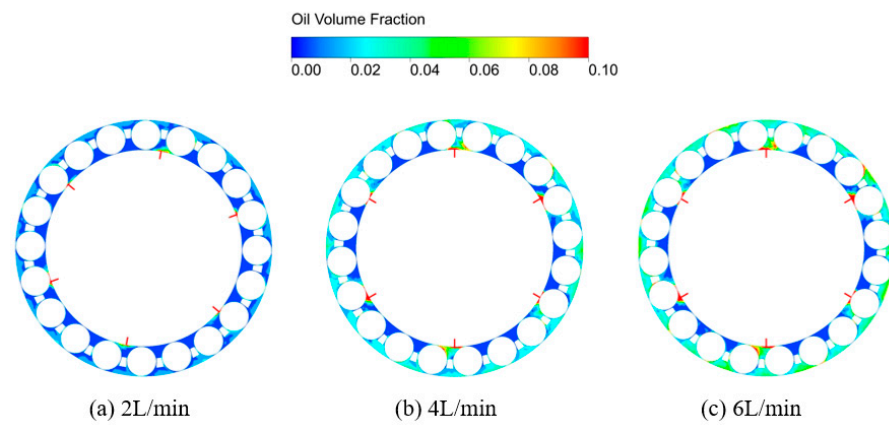


Figure 11. Oil and gas distribution at different oil volume flow rates.

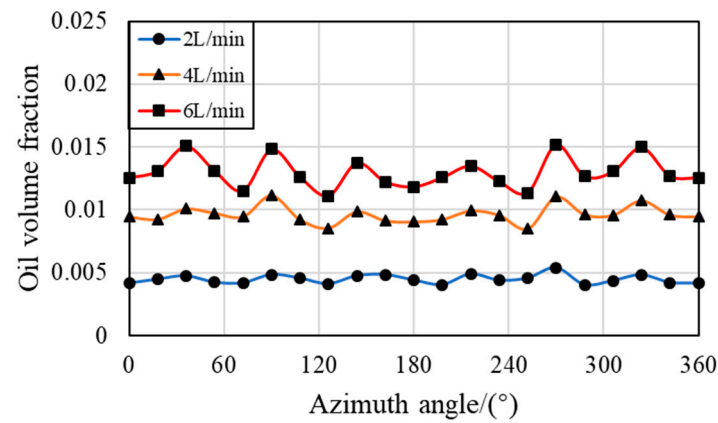


Figure 12. Circumferential oil volume fraction at different oil volume flow rates.

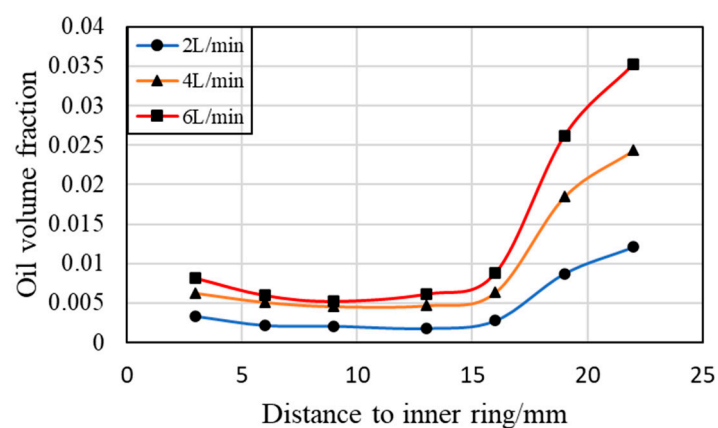


Figure 13. Radial oil volume fraction at different oil volume flow rates.

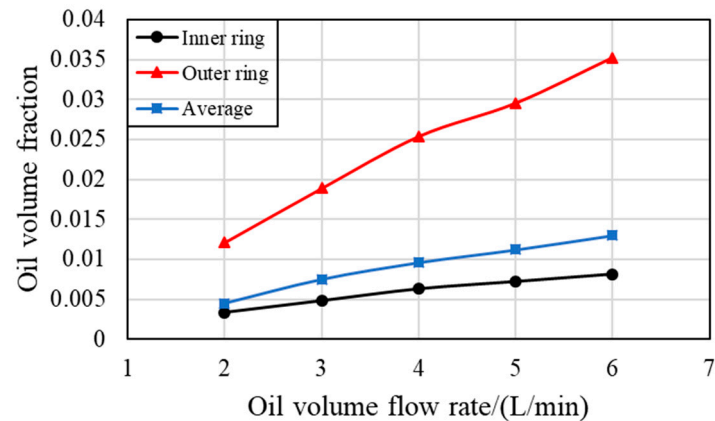


Figure 14. Oil volume fraction near the zone of the inner ring and outer rings at different oil volume flow rates.

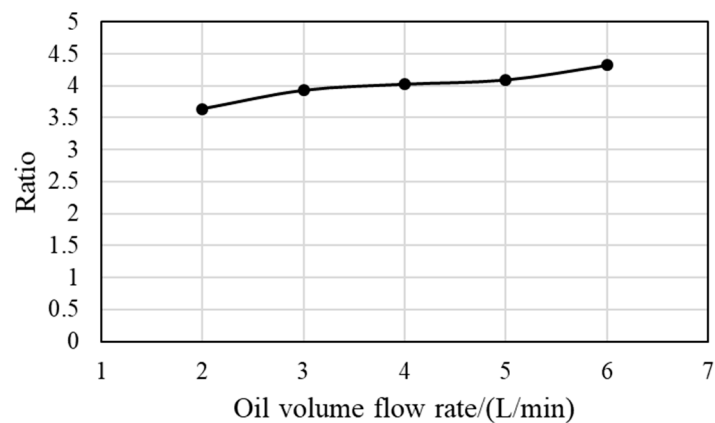


Figure 15. The ratio of oil volume fraction between the zone of the outer and inner ring at different oil volume flow rates.

3.4. The Effect of Oil Viscosity

The viscosity has a significant impact on the flow performance of oil. As shown in Figure 16, the oil-gas two-phase distribution inside the bearing at different oil viscosities is presented. The bearing rotating speed is 11,000 rpm, the oil flow rate is 3 L/min, and the oil density is 938.6 kg/m^3 . With the increase of oil viscosity, the volume fraction of the oil phase inside the bearing slightly increases and remains concentrated near the outer ring. The circumferential distribution of the oil phase inside the bearing tends to be more uniform as the oil viscosity increases, as shown in Figure 17. As shown in Figures 18 and 19, with the increase of oil viscosity, the volume fractions of the oil phase near the inner and outer rings of the bearing, as well as the average volume fraction of the oil phase inside the bearing, all increase. More oil gathers near the outer ring of the bearing. However, compared to the bearing rotating speed and oil flow rate, the oil viscosity has a less significant impact on the volume fraction of the oil phase inside the bearing. There is a trend of decreasing and then increasing differences in oil distribution between the inner and outer rings of the bearing (Figure 20). The decrease in oil viscosity will affect the lubrication effect of the bearing, and the increase in oil viscosity will lead to the increase of fluid viscous friction. Therefore, the viscosity of lubricating oil should also be kept in a reasonable range.

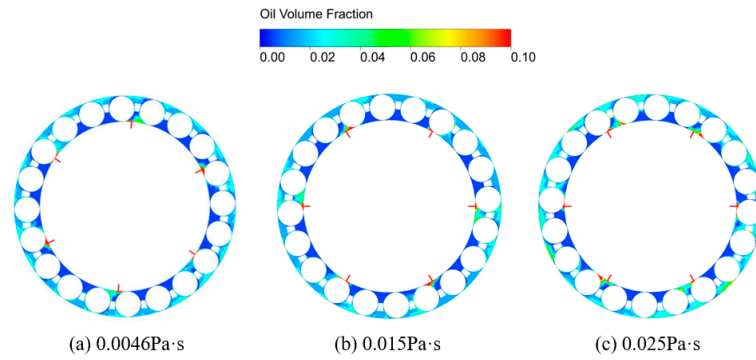


Figure 16. Oil and gas distribution at different oil viscosities.

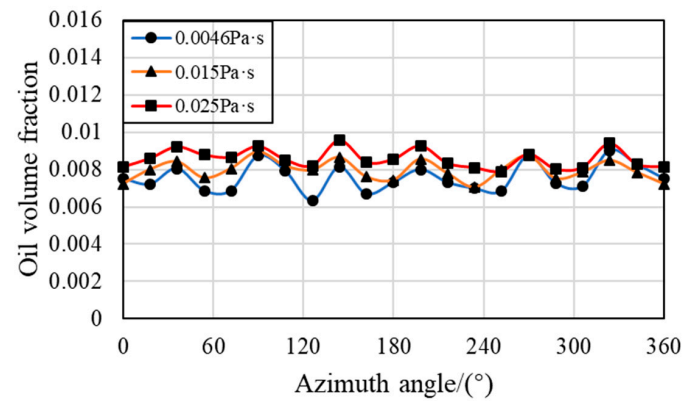


Figure 17. Circumferential oil volume fraction at different oil viscosities.

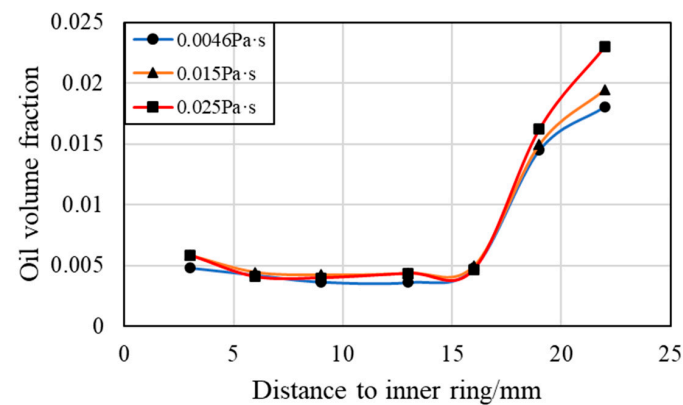


Figure 18. Radial oil volume fraction at different oil viscosities.

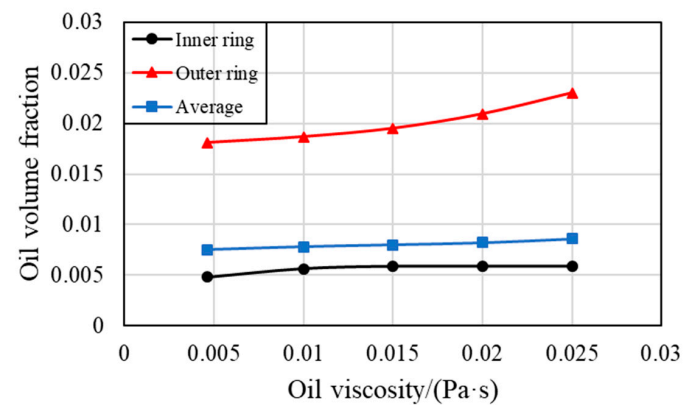


Figure 19. Oil volume fraction near the zone of the inner ring and outer rings at different oil viscosities.

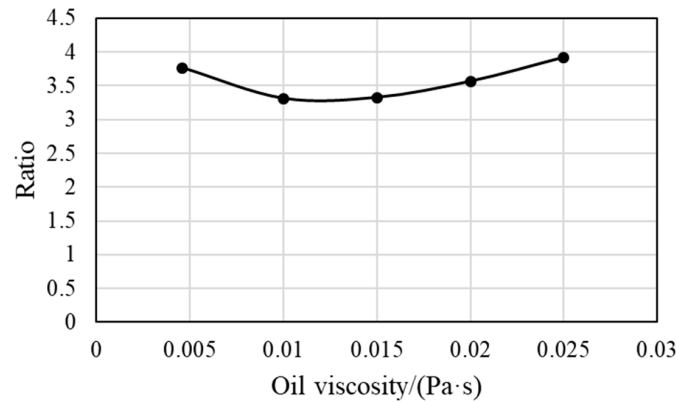


Figure 20. The ratio of oil volume fraction between the zone of the outer and inner ring at different oil viscosities.

3.5. The Effect of Oil Density

Even under large pressure and temperature variations, the density of oil does not change significantly. Within this range, the oil-gas two-phase distribution inside the bearing remains unchanged, as shown in Figure 21. The bearing rotating speed is 11,000 rpm, the oil flow rate is 3 L/min, and the oil viscosity is 0.0046 Pa·s. Within the range of oil density variations, the distribution of the oil phase inside the bearing remains basically unchanged, including circumferential distribution (Figure 22) and radial distribution (Figures 23 and 24), with the oil phase volume fraction of the outer ring being approximately 3.71 times that of the inner ring. (Figure 25)

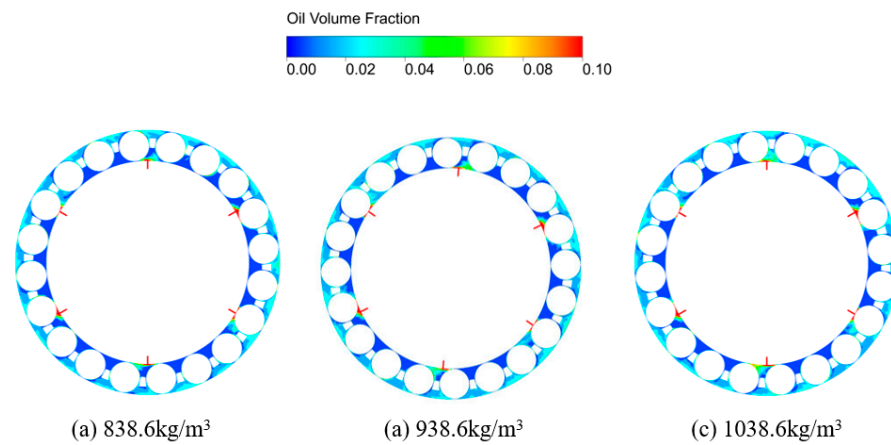


Figure 21. Oil and gas distribution at different oil densities.

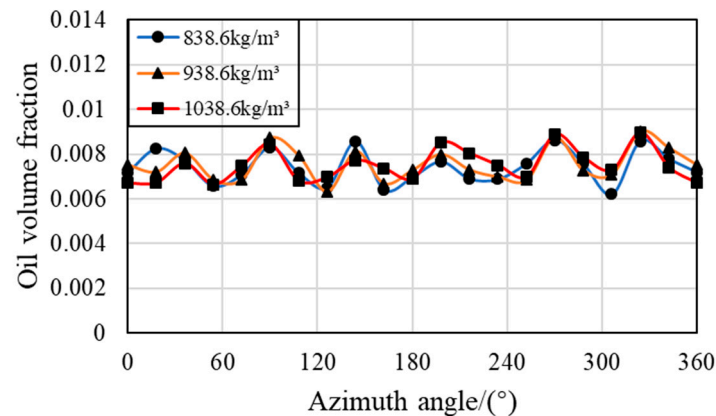


Figure 22. Circumferential oil volume fraction at different oil densities.

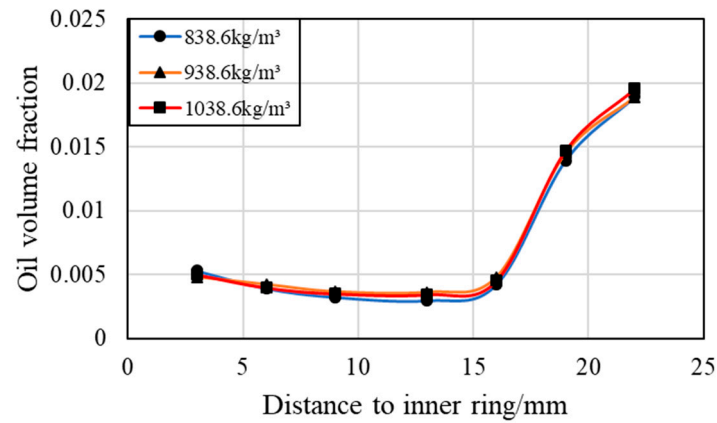


Figure 23. Radial oil volume fraction at different oil densities.

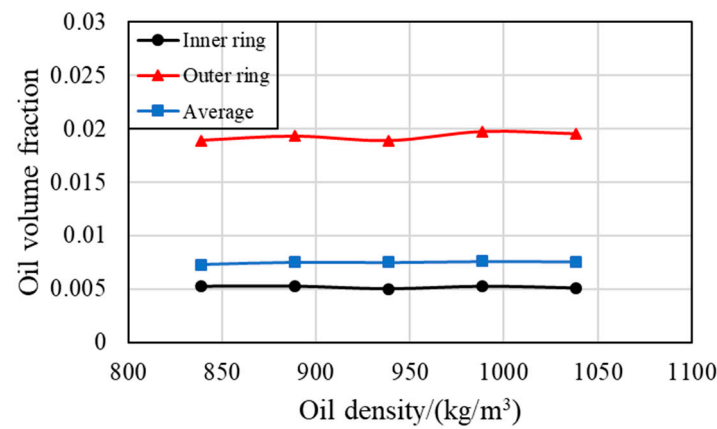


Figure 24. Oil volume fraction near the zone of inner ring and outer rings at different oil densities.

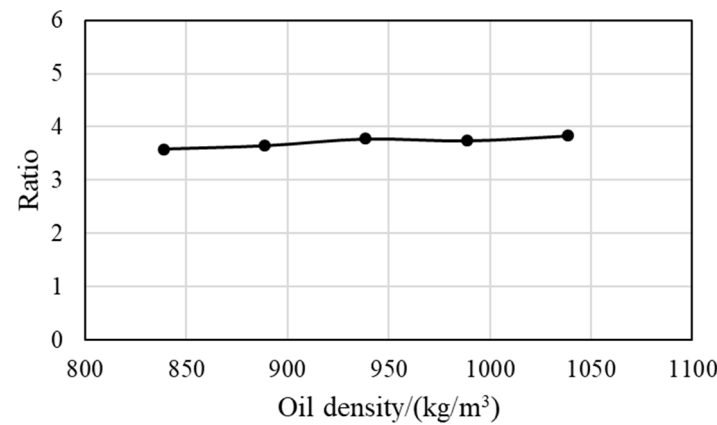


Figure 25. The ratio of oil volume fraction between the zone of the outer and inner ring at different oil densities.

3.6. Fitting of the Formula for the Average Oil Volume Percent Inside the Bearing

The average oil volume percent inside the bearing is the basis for judging the lubrication state of the bearing and is also the foundation for analyzing the fluid viscosity friction of the bearing. In order to predict the oil distribution inside the under-race lubrication ball bearing at different operating conditions, a multiple linear regression method is used to fit and establish an estimation method for the average oil volume percent in the bearing ring cavity. Through the above analysis, due to the insignificant impact of oil density changes on the average oil volume percent, only the effects of three sensitive parameters,

namely bearing rotating speed, oil flow rate, and oil viscosity, were considered. The fitted expression is as follows:

$$X_{oil} = 1593 \frac{Q^{0.949} \mu^{0.117}}{N^{0.875}} \quad (14)$$

where X_{oil} is the average oil volume percent inside the bearing; Q is the oil flow rate, expressed in L/min; μ is the oil viscosity, expressed in Pa·s; N is the bearing rotating speed, expressed in rpm.

As shown in Figure 26, this is a comparison of the calculated results obtained using the formulas mentioned in this paper with those in references Parker's [12] and Cavallaro's [13]. It can be seen from the figure that the results obtained using Parker's [12] formula are higher than those obtained using the other two formulas. This is because Parker's [12] formula provides an estimation expression for the average oil volume percent inside jet lubrication ball bearings, while Cavallaro's [13] formula is more suitable for under-race lubrication bearings. In this case, the expression provided in this paper is considered reliable as it is in close agreement with Cavallaro's [13] formula.

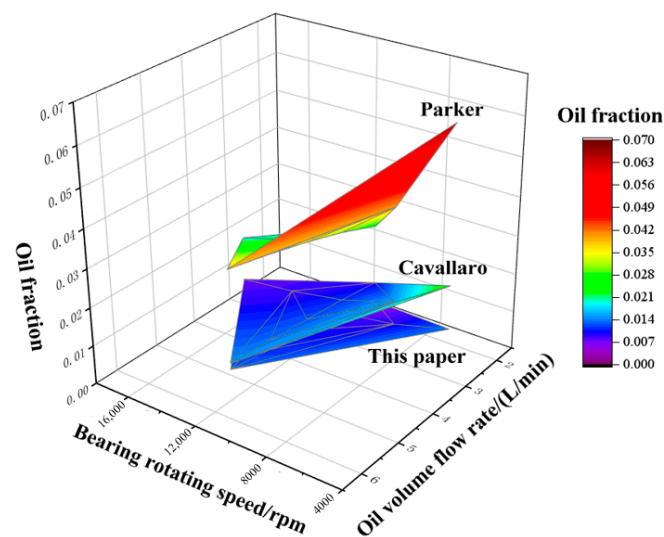


Figure 26. Oil fraction results.

4. Conclusions

In this paper, the problem of oil-gas two-phase flow inside the under-race lubrication ball bearing is studied using numerical simulation. The effects of factors such as bearing rotating speed, oil flow rate, oil viscosity, and oil density on the oil-gas two-phase distribution and average oil volume percent inside the bearing are investigated. Finally, a numerical analysis-based calculation method for the average oil volume percent inside the ring-race lubrication ball bearing is developed. The following conclusions are drawn:

- (1) In the under-race lubrication ball bearing, the oil phase exhibits a periodic distribution along the circumference, with a period that is equal to the number of supply holes. The oil phase is more abundant near the supply holes and decreases in abundance as it moves away from them. In the radial direction, due to the centrifugal force and the outer ring guiding cage, the oil phase is mainly concentrated near the outer ring.
- (2) With the increase of bearing rotating speed, the oil phase tends to distribute more evenly in both the circumferential and radial directions inside the bearing. As the oil flow rate increases, the oil within the bearing exhibits greater fluctuation in both the circumferential and radial directions. As the oil viscosity increases, the oil distributes more evenly in the circumferential direction, but the radial distribution uniformity decreases. Oil density does not significantly alter the oil distribution characteristics within the bearing.

- (3) With the increase of bearing rotating speed, the oil phase volume fractions near the inner and outer rings of the bearing gradually decrease. The increase in oil flow rate will gradually increase the volume fraction of the oil phase near the inner and outer rings of the bearing, with more oil accumulating around the outer ring compared to the inner ring. The increase of oil viscosity will also increase the accumulation of oil phase near the inner and outer rings of the bearing, but the difference in oil phase between the two regions experiences a process of first decreasing and then increasing. The oil density basically does not change the oil phase distribution near the inner and outer rings.
- (4) The average oil volume percent in the bearing ring cavity is primarily influenced by three parameters: bearing rotating speed, oil flow rate, and oil viscosity. The change in oil density has a relatively small range and can be neglected when estimating the average oil volume percent.

Author Contributions: Conceptualization, Y.L. (Yaguo Lyu) and Y.L. (Yuanhao Li); methodology, Y.L. (Yaguo Lyu); software, Y.L. (Yuanhao Li); validation, Y.L. (Yaguo Lyu), Y.L. (Yuanhao Li), L.J. and C.L.; formal analysis, Y.L. (Yaguo Lyu); investigation, Y.L. (Yuanhao Li); resources, Z.L.; data curation, Y.L. (Yuanhao Li); writing—original draft preparation, Y.L. (Yuanhao Li); writing—review and editing, Y.L. (Yaguo Lyu); visualization, Y.L. (Yuanhao Li); supervision, Y.L. (Yaguo Lyu); project administration, Y.L. (Yaguo Lyu); funding acquisition, Y.L. (Yaguo Lyu). All authors have read and agreed to the published version of the manuscript.

Funding: The authors thank the supporting of the National Science and Technology Major Project of China (Grant number: J2019-III-0023-0067) and the Natural Science Foundation of China (Grant number: 52005409).

Institutional Review Board Statement: Not applicable.

Informed Consent Statement: Not applicable.

Data Availability Statement: The original contributions presented in the study are included in the article, further inquiries can be directed to the corresponding author.

Conflicts of Interest: The authors declare no conflicts of interest.

Notation

\dot{m}_{ao}	mass transfer rate from the gas phase to the oil phase per unit volume
\dot{m}_{oa}	mass transfer rate from the oil phase to the gas phase per unit volume
$S_{\alpha_{oil}}$	source term defined by the volume fraction equation
φ_{air}	air phase volume fraction
φ_{oil}	oil phase volume fraction
$C_{1\varepsilon}, C_{2\varepsilon}$	constant terms
D	ball diameter
d_m	pitch diameter
G_k	generation of turbulent kinetic energy due to mean velocity gradients
k	turbulent kinetic energy
n_i	inner ring speed
n_m	cage speed
n_{mi}	rotating speed of cage relative to inner ring
n_r	ball's self-rotation speed
v_m	cage linear velocity
α	contact angle
ε	turbulent dissipation
μ_{oil}	oil viscosity
μ_{air}	air viscosity
μ_{eff}	effective dynamic viscosity
μ_i	time-averaged velocity
μ_t	turbulent viscosity

ρ_{air}	air density
ρ_{oil}	oil density
ω_m	cage angular velocity
ω_r	ball angular velocity

References

- Gloeckner, P.; Rodway, C. The Evolution of Reliability and Efficiency of Aerospace Bearing Systems. *Engineering* **2017**, *9*, 962–991. [[CrossRef](#)]
- Gloeckner, P.; Dullenkopf, K.; Flouros, M. Direct Outer Ring Cooling of a High-speed Jet Engine Mainshaft Ball Bearing: Experimental Investigation Results. *J. Eng. Gas Turbines Power* **2011**, *133*, 80–86. [[CrossRef](#)]
- Milan, B.; Sandra, G.; Aleksandar, S.; Slobodan, S.; Aleksandar, A.; Blaza, S. Tribological Application of Nanocomposite Additives in Industrial Oils. *Lubricants* **2024**, *12*, 6.
- Gao, W.; Nelias, D.; Boisson, N.; Lyu, Y. Model Formulation of Churning Losses in Cylindrical Roller Bearings Based on Numerical Simulation. *Tribol. Int.* **2018**, *121*, 420–434. [[CrossRef](#)]
- Pinel, S.I.; Signer, H.R.; Zaretsky, E.V. Comparison between Oil-Mist and Oil-Jet Lubrication of High-Speed, Small-Bore, Angular-Contact Ball Bearings. *Tribol. Trans.* **2001**, *44*, 327–338. [[CrossRef](#)]
- Paloma, C.; Kathy, S.; Arun, P.; Budi, C. Assessment of the Oil Scoop Capture Efficiency in High-speed Rotors. *J. Eng. Gas Turbines Power* **2019**, *141*, 012401.
- Jiang, L.; Liu, Z.; Lyu, Y.; Qin, J. Numerical Simulation on the Oil Capture Performance of the Oil Scoop in the Under-Race Lubrication System. *Proc. Inst. Mech. Eng. Part G J. Aerosp. Eng.* **2021**, *235*, 2258–2273. [[CrossRef](#)]
- Wu, W.; Hu, C.; Hu, J.; Yuan, S.; Zhang, R. Jet Cooling Characteristics for Ball Bearings Using the VOF Multiphase Model. *Int. J. Therm. Sci.* **2017**, *116*, 150–158. [[CrossRef](#)]
- Zaretsky, E.V.; Bamberger, E.N.; Signer, H.R. *Operating Characteristics of 120-Millimeter-Bore Ball Bearing at 3 Million*; NASA TN D-7837; NASA: Washington, DC, USA, 1974.
- Pinel, S.I.; Signer, H.R.; Zaretsky, E.V. Design and Operating Characteristics of High-Speed, Small-Bore Ball Bearings. *Tribol. Trans.* **1998**, *41*, 423–434. [[CrossRef](#)]
- Pinel, S.I.; Signer, H.R.; Zaretsky, E.V. Design and Operating Characteristics of High-Speed, Small-Bore Cylindrical-Roller Bearings. *Tribol. Trans.* **2001**, *44*, 70–78. [[CrossRef](#)]
- Parker, R.J. *Comparison of Predicted and Experimental Thermal Performance of Angular-Contact Ball Bearings*; NASA Technical Paper 2275; NASA: Washington, DC, USA, 1984.
- Cavallaro, G.; Nelias, D.; Bon, F. Analysis of High-Speed Intershaft Cylindrical Roller Bearing with Flexible Rings. *Tribol. Lubr. Technol.* **2005**, *48*, 154–164. [[CrossRef](#)]
- Hu, J.; Wu, W.; Wu, M.; Yuan, S. Numerical Investigation of the Air–Oil Two-Phase Flow Inside an Oil-Jet Lubricated Ball Bearing. *Int. J. Heat Mass Transf.* **2014**, *68*, 85–93. [[CrossRef](#)]
- Liebrecht, J.; Si, X.; Sauer, B.; Schwarze, H. Investigation of Drag and Churning Losses on Tapered Roller Bearings. *J. Mech. Eng.* **2015**, *61*, 399–408. [[CrossRef](#)]
- Zhang, R.; Wei, C.; Wu, W.; Yuan, S. CFD Investigation on the Influence of Jet Velocity of Oil-Jet Lubricated Ball Bearing on the Characteristics of Lubrication Flow Field. In Proceedings of the 2015 International Conference on Fluid Power and Mechatronics (FPM), Harbin, China, 5–7 August 2015; pp. 1324–1328.
- Adeniyi, A.A.; Morvan, H.P.; Simmons, K.A. A CFD Simulation of Oil–Air Flow Between the Cage and Inner Race of an Aeroengine Bearing. *J. Eng. Gas Turbines Power* **2016**, *139*, 012506. [[CrossRef](#)]
- Yuan, S.; Hu, C.; Hu, J.; Wu, W. Jet Cooling for Rolling Bearings: Flow Visualization and Temperature Distribution. *Appl. Therm. Eng.* **2016**, *105*, 217–224.
- Yan, K.; Wang, Y.; Zhu, Y.; Hong, J. Investigation on the Effect of Sealing Condition on the Internal Flow Pattern of High-Speed Ball Bearing. *Tribol. Int.* **2017**, *105*, 85–93. [[CrossRef](#)]
- Gao, W.; Nelias, D.; Li, K.; Liu, Z.; Lyu, Y. A Multiphase Computational Study of Oil Distribution Inside Roller Bearings with Under-Race Lubrication. *Tribol. Int.* **2019**, *140*, 105862. [[CrossRef](#)]
- Jiang, L.; Lyu, Y.; Gao, W.; Zhu, P.; Liu, Z. Numerical Investigation of the Oil–Air Distribution Inside Ball Bearings with Under-Race Lubrication. *Proc. Inst. Mech. Eng. Part J J. Eng. Tribol.* **2022**, *236*, 499–513. [[CrossRef](#)]
- Hirt, C.W.; Nichols, B.D. Volume of Fluid (VOF) Method for the Dynamics of Free Boundaries. *J. Comput. Phys.* **1981**, *39*, 201–225. [[CrossRef](#)]
- Xiao, J.; Zhu, E.; Wang, G. Numerical Simulation of Emergency Shutdown Process of Ring Gate in Hydraulic Turbine Runaway. *J. Fluids Eng.* **2012**, *134*, 124501. [[CrossRef](#)]
- Lynagh, N.; Rahnejat, H.; Ebrahimi, M.; Aini, R. Bearing induced vibration in precision high-speed routing spindles. *Int. J. Mach. Tools Manuf.* **2000**, *40*, 561–577. [[CrossRef](#)]

Disclaimer/Publisher’s Note: The statements, opinions and data contained in all publications are solely those of the individual author(s) and contributor(s) and not of MDPI and/or the editor(s). MDPI and/or the editor(s) disclaim responsibility for any injury to people or property resulting from any ideas, methods, instructions or products referred to in the content.